Charmonium suppression from shadowing effects

N. Hammon, L. Gerland, H. Stöcker, and W. Greiner
Institut Für Theoretische Physik, Robert-Mayer Strasse 10, Johann Wolfgang Goethe-Universität, D-60054 Frankfurt am Main, Germany
(Received 30 July 1998; revised manuscript received 29 October 1998)

The extent to which geometrical effects contribute to the production and suppression of the J/ψ and $q\bar{q}$ minijet pairs in general is investigated for high-energy heavy-ion collisions at SPS, RHIC, and LHC energies. For the energy range under investigation, the geometrical effects referred to are shadowing and antishadowing, respectively. Due to those effects, the parton distributions in nuclei deviate from the naive extrapolation from the free nucleon result; $f_A \neq A f_N$. The strength of the shadowing/antishadowing effect increases with the mass number. Therefore it is interesting to see the difference between cross sections for, e.g., $S+U$ vs Pb+Pb at SPS. The recent NA50 results for the survival probability of produced J/ψ's has attracted great attention and are often interpreted as a signature of a quark gluon plasma. This paper will present a fresh look on hard QCD effects for the *charmonium production* level. It is shown that the apparent suppression of J/ψ's must also be linked to the production process. Due to the uncertainty in the shadowing of gluons the suppression of charmonium states might not give reliable information on a created plasma phase at the collider energies now available. The consequences of shadowing effects for the x_F distribution of J/ψ's at $\sqrt{s}=20$ GeV, $\sqrt{s}=200$ GeV, and $\sqrt{s}=6$ TeV are calculated for some relevant combinations of nuclei, as well as the p_T distribution of minijets at midrapidity for $N_f=4$ in the final state. [S0556-2813(99)04205-3]

PACS number(s): 24.85.+p, 14.40.Lb, 25.75.−q

I. INTRODUCTION

Since the advent of QCD in the 1970s great emphasis was laid on the existence of a phase transition of, yet unknown, order, being typical for non-Abelian gauge-field theories. From lattice calculations it was emphasized that, at zero chemical potential, a phase transition should show up at some temperature $T_c \approx 150-200$ MeV when explicitly taking quarks into account. The value for T_c is slightly higher for a pure gauge theory. Also, at the nonzero chemical potential, as suggested in the MIT bag model, one should access a phase transition due to the increasing outward pressure of the partons inside the bag finally leading to a deconfined phase. Due to the difficulties emerging when considering dynamical fermions, the work on a nonzero chemical potential has not yet reached the same level of success as that for $\mu=0$ in lattice QCD.

Now, in actual high-energy heavy-ion collisions the following scenario can occur. Two streams of initially cold nuclear matter collide and may result in a plasma phase, which is created within the transverse dimension of approximately the size of the overlapping nuclei. The plasma cools down to form hadronic degrees of freedom in the subsequent expansion. If one has this phase transition in mind one also has to confront the question of its experimenatal detection. Typical signatures under discussion are leptonic (dilepton [1] and photon [2] production due to the interactions among the quasifree partons via the different QCD processes $q\bar{q}\rightarrow\gamma g$, $gq\rightarrow\gamma q$, ...) and hadronic ones, such as the suppression of J/ψ's. Now, the QCD reactions in the plasma are not the only source for leptons. One expects a large background coming from the decay of π^0 and η mesons. It therefore is necessary to carefully handle this background by experimental methods such as invariant mass analysis.

It is also obvious that the signatures have to give clear and powerful information on the plasma phase. Especially when looking at the hadronic signatures this does not have to be the case as emphasized in [3], where it was shown that gluon depletion due to DGLAP splitting in the colliding nuclei can lead to the same results as the current experiments at NA50 [4], which in turn implies that those experimental results probably have lost their meaning as a plasma signature at SPS.

II. PRODUCTION AND SUPPRESSION OF THE J/ψ

The J/ψ is a $c\bar{c}$ bound state interacting via two forces in a confined surrounding: a linear confining potential and a color-Coulomb interaction. In the plasma phase the linear potential is absent due to the high temperature leading to deconfinement. Every color charge is Debye screened by a cloud of surrounding quark-antiquark pairs which weaken the binding force between the $c\bar{c}$ pair, thus reducing the color charge seen by the other (anti)quark. Since the density of the screening pairs rises strongly with increasing temperature, the binding force gets weaker and weaker when the temperature rises above T_c. As a result, the charm quark and antiquark drift away from each other, so that finally no bound-state formation is possible in a plasma phase of high enough temperature [5].

However, the plasma phase is not the only source of suppression [6]. One also has to take into account final-state interactions for this hadronic degree of freedom, which are absent for leptonic signatures. Because the J/ψ is a very weakly bound state, the interaction with nucleons and secondaries that are always present in a heavy-ion collision, in addition, significantly lowers the survival propability for a J/ψ. It is obvious that such effects should increase with increasing mass number. One also expects the phase transition to happen for the heavier nuclei. Therefore, one has two

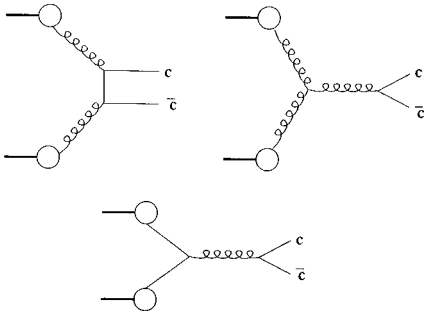

FIG. 1. The various LO processes leading to the direct production of a $c\bar{c}$ pair.

effects both increasing with the number of nucleons involved. This in turn implies that the experiments have to be done with very high precision to disentangle those effects.

At this point another source of suppression comes into play that also increases with the mass number and therefore has to be accounted for: *nuclear shadowing*. This effect already enters on the production level of the charmonium bound state. The former two effects, namely suppression by melting in the plasma phase and comover activity, enter only at a level when the J/ψ already exists at later proper times τ. Now the nuclear shadowing effect appears when the charmonium is produced via the various processes depicted in Fig. 1.

The total hidden charm cross section in pN collisions below the open charm threshhold is given by [7]

$$\sigma_{c\bar{c}}(s)=\int_{4m_c^2}^{4m_D^2} d\hat{s}\int dx_A dx_B f_i(x_A) f_j(x_B)\hat{\sigma}(\hat{s})\,\delta(\hat{s}-x_A x_B s). \tag{1}$$

Here, f_i and f_j denote the parton densities and $\hat{\sigma}$ is the cross section on the parton level, i.e., $q\bar{q}\to c\bar{c}$, $gg\to c\bar{c}$. The $c\bar{c}$ pair subsequently will turn into a color singlet by interaction with the color field induced in the scattering, the so-called ''color-evaporation'' mechanism. In [7] the J/ψ production in a proton nucleon reaction was parametrized as

$$\sigma_{pN\to J/\psi}(s)=f^p_{J/\psi}\sigma^{\mathrm{NLO}}_{c\bar{c}} \tag{2}$$

with $f^p_{J/\psi}=0.025$ from comparison with data [8]. Here the production of the J/ψ is described as proceeding via the NLO production of a $c\bar{c}g$ state and the subsequent evaporation of the gluon. (For a more detailed model also including the non-relativistic quarkonium model in the quarkonium- and bottonium-nucleon cross section see [9].)

It is obvious that any changes in the parton densities will result in changes of the $c\bar{c}$ production cross section. Because we know since the EMC measurements [10] that $f_i^A\neq Af_i^N$ this demands some further investigation. Here we will investigate the influence of the *nuclear gluon and quark distributions* on the J/ψ production cross section by using a modified version of a parametrization based on a (impact parameter averaged) data fit given in [11]. We will show the influence on the differential cross section $d\sigma^{AB}/dx_F$ for gg fusion and $q\bar{q}$ annihilation [12] given by

$$\frac{d\sigma^{AB}_{gg}}{dx_F}=\int_{4m_c^2}^{4m_D^2} dQ^2\,\frac{1}{Q^2}\,\frac{x_A x_B}{x_A+x_B}\hat{\sigma}^{gg\to c\bar{c}}(Q^2) \times g^A(x_A,Q^2)g^B(x_B,Q^2), \tag{3}$$

$$\frac{d\sigma^{AB}_{q\bar{q}}}{dx_F}=\sum_{q=u,d,s}\int_{4m_c^2}^{4m_D^2} dQ^2\,\frac{1}{Q^2}\,\frac{x_A x_B}{x_A+x_B}\hat{\sigma}^{q\bar{q}\to c\bar{c}}(Q^2) \times[q^A(x_A,Q^2)\bar{q}^B(x_B,Q^2)+q\leftrightarrow\bar{q}], \tag{4}$$

and on the minijet cross section

$$\frac{d\sigma}{p_T dp_T dy_1 dy_2}=2\pi x_A g^A(x_A,p_T^2)x_B g^B(x_B,p_T^2)\frac{d\hat{\sigma}^{gg\to q\bar{q}}}{d\hat{t}} \tag{5}$$

at midrapidity $y=y_1=y_2=0$. We choose $m_c=1.5$ GeV and $m_D=1.85$ GeV. The momentum fractions are given as $x_{A,B}=1/2[\pm x_F+(x_F^2+4Q^2/s)^{1/2}]$ for the x_F distribution and $x=2p_T/\sqrt{s}$ for the minijets at midrapidity. We take all cross sections in leading order and do not include any K factor for higher-order contributions since we are mainly interested in relative effects. For the parton distributions we choose the CTEQ4L parametrization.

The reason for our investigation is the following: the recent NA50 data show a deviation from the tendency expected from earlier experiments when the mass number of the involved nuclei is increased. Now, in [3] it was shown that due to multiple scatterings between partons the uncertainty in the survival propability gets so large that one cannot distinguish whether the data found by NA50 is due to gluon splitting in the production phase or due to plasma absorption as claimed by several authors. Obviously, the originally good idea of J/ψ suppression as a good tool for plasma investigation seems to have lost its predictive power at the available energies. It is therefore interesting to see what one can expect at future colliders.

In the next part we will give some details of the parton densities in nuclei in the energy regimes of SPS, RHIC, and LHC.

III. NUCLEAR SHADOWING AND THE CONNECTION TO THE J/ψ

The history of the modification of nuclear structure functions, as compared to the free nucleon ones, is founded on the findings of the EMC group that lead to the so-called EMC effect [10] (even though one should say that shadowing effects, in principle, have been known since the 1970s [13]). This effect shows that $f_A\neq Af_N$, which implies that the parton density in the nucleus is not simply given by the nucleon number times the respective parton density in the nucleon. Depending on the frame (lab- or infinite momentum frame) one derives completely different interpretations for the nuclear structure functions and for the deviations from the naive pp extrapolations. For typical values of the momentum transfer in a pp reaction of $p_T=1-6$ GeV, where perturbation theory should be applicable, one is in the so-called antishadowing region for SPS and in the shadowing region for RHIC and LHC at midrapidity. In the following

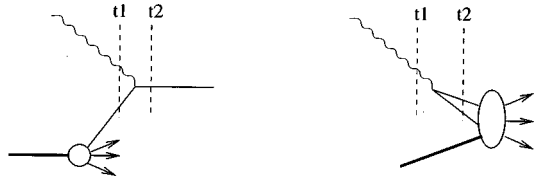

FIG. 2. The two physical processes arising from the two possible time orderings.

we will shortly review the interpretation of shadowing in the two relevant frames and will start with the lab frame description which is the *natural* frame for typical deep inelastic-scattering measurements off nuclei (at least from the experimental setup point of view).

A. Lab frame description

In the lab frame the expression *shadowing* immediately seems to imply a geometrical effect. When one speaks of something lying in the shadow of another thing one means that the second body is not visible since the first body is placed nearer, e.g., to some source of light. A similar reasoning can be applied in the case when a lepton is scattered off a nucleus consisting of many nucleons. The exchanged virtual photon does not (in the relevant x range) interact individually with each nucleon but coherently with all nucleons or at least with a major part of the nucleons inside the nucleus; some nucleons are therefore lying *in the shadow* of other (surface) nucleons. As we will see later, this reasoning is linked to the momentum fraction of the struck parton inside the nucleon. Because the momentum fraction is bound from above this interpretation is limited to the explanation of shadowing and is not applicable for the reasoning of antishadowing, the EMC effect or the Fermi-motion effect. Unfortunately there is yet no single theory to understand the whole range of the momentum fraction from $0 \leqslant x_{Bj.} \leqslant 1$. For an excellent review of different models and interpretations see [14].

For a deep inelastic-scattering process there exist two possible time orderings for the interaction of a virtual photon with a nucleon or with a nucleus: either the photon hits a quark inside the target (the so-called hand-bag graph) or the photon creates a $q\bar{q}$ pair which then strongly interacts with the target. Those two possible processes are depicted in Fig. 2.

As can be seen from the ratio of the amplitudes of the two processes one realizes that the diagram on the right-hand side only contributes at small enough x ($x \ll 0.1$). At low Q^2 the interaction of the virtual photon with the nucleons inside the nucleus happens via the low mass vector mesons ρ, ω, and ϕ as described in the vector meson dominance model (VMD) with the typical spectral ansatz for the description of the fluctuation spectrum [15]. The reduction in the quark density, manifesting itself in the shadowing ratio $R_{F_2} = F_2^A/A \cdot F_2^N$, can then be understood in terms of a multiple scattering series where the fluctuation interacts with more than one nucleon over a coherence length of $l_c \approx 1/(2mx)$. At higher Q^2 the partonic degrees of freedom are probed; nevertheless, shadowing is due to long distance effects and therefore always incorporates a strong nonperturbative component, even at large Q^2. Also, the $q\bar{q}$ continuum has to be taken in addition to the mesons giving rise to the generalized VMD model.

The interaction of the virtual photon with a nucleon can essentially be split up into two parts: the virtual photon with its quark-antiquark fluctuation and the interaction of the fluctuation with the parton which happens via gluon exchange:

$$\sigma(\gamma^* N) = \int_0^1 dz \int d^2r |\psi(z,r)|^2 \sigma_{q\bar{q}N}(r), \tag{6}$$

where the Sudakov variable z gives the momentum fraction carried by the quark (or antiquark).

The cross section for the interaction of the fluctuation with the nucleon can be described in the ''double log approximation''

$$\sigma_{q\bar{q}N} = \frac{\pi^2}{3} r^2 \alpha_s(Q'^2) x' g(x', Q'^2), \tag{7}$$

where $x' = M_{q\bar{q}}^2/(2m\nu)$, r is the transverse separation of the pair, and $Q'^2 = 4/r^2$. Due to

$$|\psi(z,r)| \sim \frac{1}{r^2}, \tag{8}$$

pairs with small transverse separation are favored. As can be seen from Eq. (7) this in turn implies a small cross section. This smallness is compensated by the strong scaling violation of the gluon distribution in the small x region as r (Q'^2) decreases (increases). In the Glauber eikonal approximation the interaction with the nucleus is expressed in terms of the nuclear thickness function $T_A(b)$ as

$$\sigma_{q\bar{q}A} = \int d^2b (1 - e^{-\sigma_{q\bar{q}N} T_A(b)/2}). \tag{9}$$

When there is a longitudinal momentum transfer appropriate to the production of the hadronic fluctuation h, a phase shift behind the target results and the incident wave $\exp(ik_z^\gamma z)$ is changed to $-\Gamma(b)\exp(ik_z^h z)$ with $k_z^\gamma \neq k_z^h$ and the nucleus profile function $\Gamma(b)$. The phase shift $\Delta k_z = k_z^\gamma - k_z^h$ in turn gives rise to the coherence length $l_c \approx 1/\Delta k_z$. When now $l_c \gg 2R_A$ (i.e., for small momentum transfers Δk_z), the hadronic fluctuation interacts coherently with all nucleons inside the nucleus, Glauber theory is valid and a reduction in the cross section results (for further details we refer to [14–17]). For an illustration of the effect, see Fig. 3.

B. Infinite momentum frame description

In the infinite momentum frame a completely different mechanism is employed. The key idea here is the fusion of partons giving rise to a process that competes with parton splitting expressed in the DGLAP equations. This idea was formulated in [17] and later proven in [18]. In the following we will give the main ideas and conclusions of the parton fusion model [19].

As is known, in the infinite momentum frame the Bjorken variable x_{Bj} is interpreted as the momentum fraction of a parton with respect to the mother nucleon. When now, inside

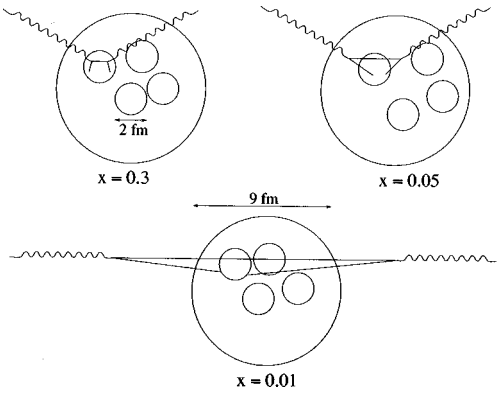

FIG. 3. Graphic representation of the lab frame interpretation of shadowing.

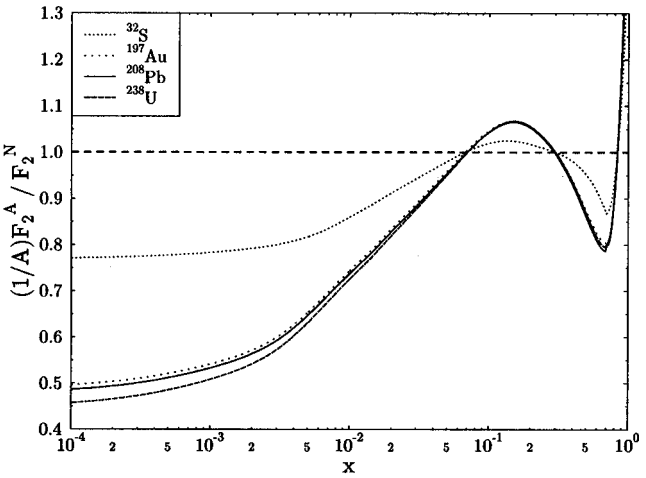

FIG. 4. Fit to the data for various nuclei at $Q_0 = 2$ GeV as given by Eskola.

a nucleus, the longitudinal wavelength of a parton exceeds the Lorentz-contracted size of a nucleon or the internucleon distance $2R_N$, then partons originating from different nucleons can ''leak out'' and fuse. This effect can be estimated from $1/(xP) \approx 2R_N M_N/P$ to show up at x values smaller than $x \approx 0.1$. As a result of the parton-parton fusion partons are ''taken away'' at smaller values of x and ''shoveled'' to larger values of x where antishadowing appears to guarantee momentum conservation. As a result of the parton fusion the x range for the measured structure function is expanded to values $x > 1$. Hereby, an alternative description of Fermi motion is achieved. In the lab frame interpretation the saturation of shadowing was interpreted in terms of a coherence length larger than the nucleus. Here, the saturation towards smaller x values is interpreted in terms of the longitudinal parton wave length exceeding the size of the nucleus. In that sense the infinite momentum frame interpretation of shadowing is formulated in terms of variables that are inherent to the nucleus and there is no need for a scattered lepton or a collision.

In addition to the longitudinal shadowing one expects an additional shadowing effect from the transverse fusion of partons: for sufficiently small values of x and/or Q^2 the total transverse occupied area of the partons becomes larger than the transverse area of the nucleon. This happens (e.g., for gluons) when $xg(x) \geqslant Q^2 R^2$ where the transverse size of a parton is $1/Q^2$ and R is the nucleon radius. The depletion in the gluon and sea-quark densities arising from that process are expected at values $x \leqslant 0.01$.

At this point some comments concerning the general influence of initial- and final-state interactions on the suppression of $c\bar{c}$ states are appropriate. The relative influence of the final-state interactions (such as comovers) to initial-state interactions (such as shadowing) changes significantly when going from SPS to RHIC and LHC.

For a Pb nucleus of $R_{\mathrm{Pb}} \approx 6.5$ fm, the passage time of the two nuclei in the c.m. system with a γ factor of $\gamma \approx 9.3$ is $t_{\mathrm{pass}} \approx 1.4$ fm/c at SPS, which is of the same order of magnitude as, e.g., meson production. The production time of a $c\bar{c}$ pair is $t_{\mathrm{prod}} \approx 0.07$ fm/c. So obviously after the production of the pair many final-state interactions can happen due to the long time it takes the two nuclei to run over the quark antiquark pair. In addition the initial-state effects are much weaker because the momentum fractions at midrapidity for the energies of $S+U$ and Pb+Pb are found in the antishadowing region or even in between the antishadowing and EMC region, depending on the energy. So taking these two aspects together one has to conclude that the influence of shadowing effects at SPS are dominated by the final-state interactions and that shadowing does not significantly contribute. However, at RHIC, the passage time becomes $t_{\mathrm{pass}} \approx 0.12$ fm/c due to the stronger Lorentz contraction. This implies that the influence of secondaries such as produced mesons tends to get smaller and the $c\bar{c}$ state has a larger chance to escape the reaction zone without too many collisions. However, the perturbative quarkonium-nucleon cross section increases with the energy as shown in the color transparency model in [20] which could balance the vanishing influence of the secondaries. When taking shadowing into account in this case $\sigma_{\mathrm{hard}}(q\bar{q}N)$ should too. So already at RHIC, the final-state interaction loses influence on the survival probability in favor of the initial-state effects that get stronger since the relevant momentum fractions are clearly in the shadowing region. This tendency increases further at LHC since the initial-state shadowing gets stronger.

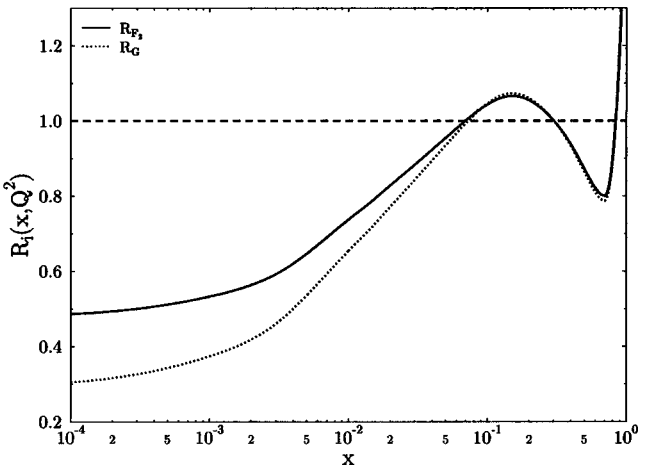

FIG. 5. Initial gluon and quark shadowing parametrization at $Q^2 = 4$ GeV^2 for ^{197}Au and ^{208}Pb.

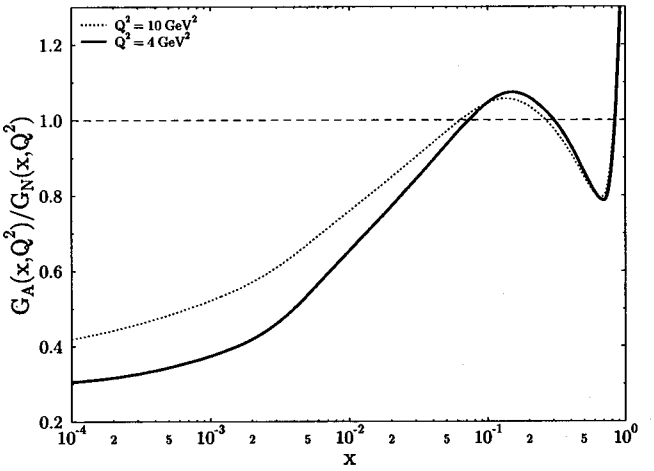

FIG. 6. Gluon shadowing ratio evolved to $Q^2=10$ GeV^2 with DGLAP without fusion terms. Due to the narrow range $4m_c^2 \leqslant Q^2 \leqslant 4m_D^2$ in the interpretation we use the ratio at some fixed intermediate scale $Q^2=10$ GeV^2.

IV. THE USED PARAMETRIZATION

In [11] a fit to the E772 [21], NMC [22], and SLAC [23] data was given as a parametrization for the ratio $R_{F_2} = F_2^A/A \cdot F_2^N$ (see Fig. 4). Now this parametrized ratio cannot simply be multiplied with all the individual parton distributions entering the formulas. One has to make a distinction between the valence and the sea quarks and also needs a different ratio for the gluons. Our results for $d\sigma^{AB}/dx_F$ are based on the shape of the ratio given in [11] at the initial momentum transfer $Q_0=2$ GeV. Up to now, the production processes were often calculated by using the measured shadowing ratio R_{F_2}. From the lab frame interpretation we know that the cross section for the interaction of a gluon pair is larger than the one for the interaction of the quark-antiquark pair ($\sigma_{ggN}^{\text{pert}} = 9/4\sigma_{q\bar{q}N}^{\text{pert}}$). The same tendency can be found in the parton fusion model. In [24] calculations in the parton fusion model for ^{118}Sn showed an impact-parameter-averaged gluon shadowing that is twice as strong ($R_G \approx 0.34$) as the sea quark shadowing at $x=10^{-3}$ and $Q^2=5$ GeV^2 already for this light nucleus. To account for the much stronger gluon shadowing we, therefore, modified the parametrization given in [11].

In the lab frame, the relevant range for the coherence length to produce the shadowing effect is $l_0 = r_{NN} \approx 1.8$ fm $\leqslant l_c = 1/(2mx) \leqslant 2R_A$. For $l_c \gg 2R_A$, corresponding to $x \ll 0.1$ fm/1.1 fm$A^{1/3}$, the shadowing of gluons at some initial scale at fixed impact parameter behaves as [25,26]

$$\frac{A_{\text{eff}}}{A} = \frac{2-2(\exp -R/2)}{R}, \tag{10}$$

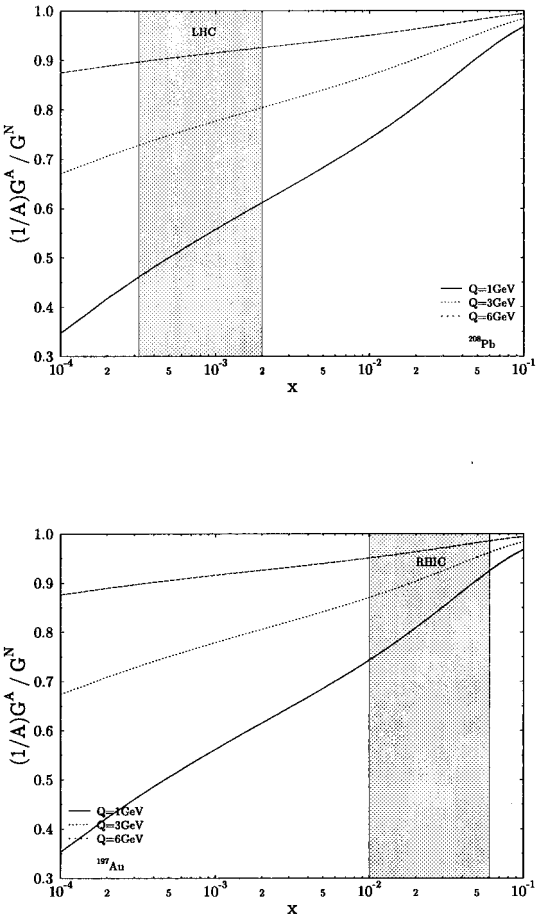

FIG. 7. Gluon ratios corresponding to the various energy and transverse momentum regimes.

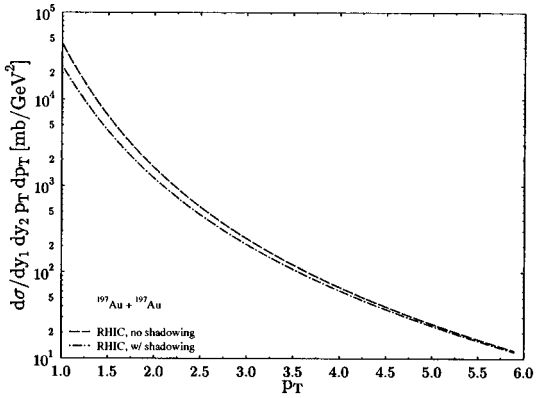

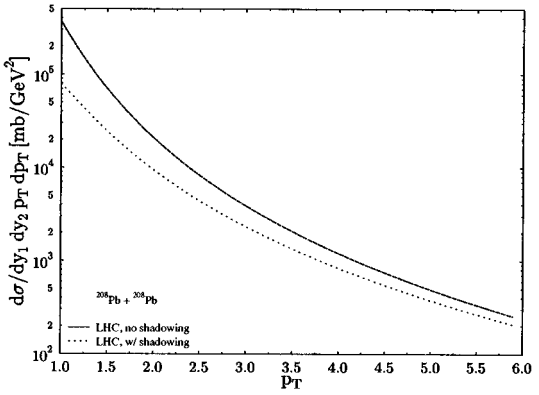

FIG. 8. Minijet cross sections for creation of $q\bar{q}$ pairs for RHIC and LHC.

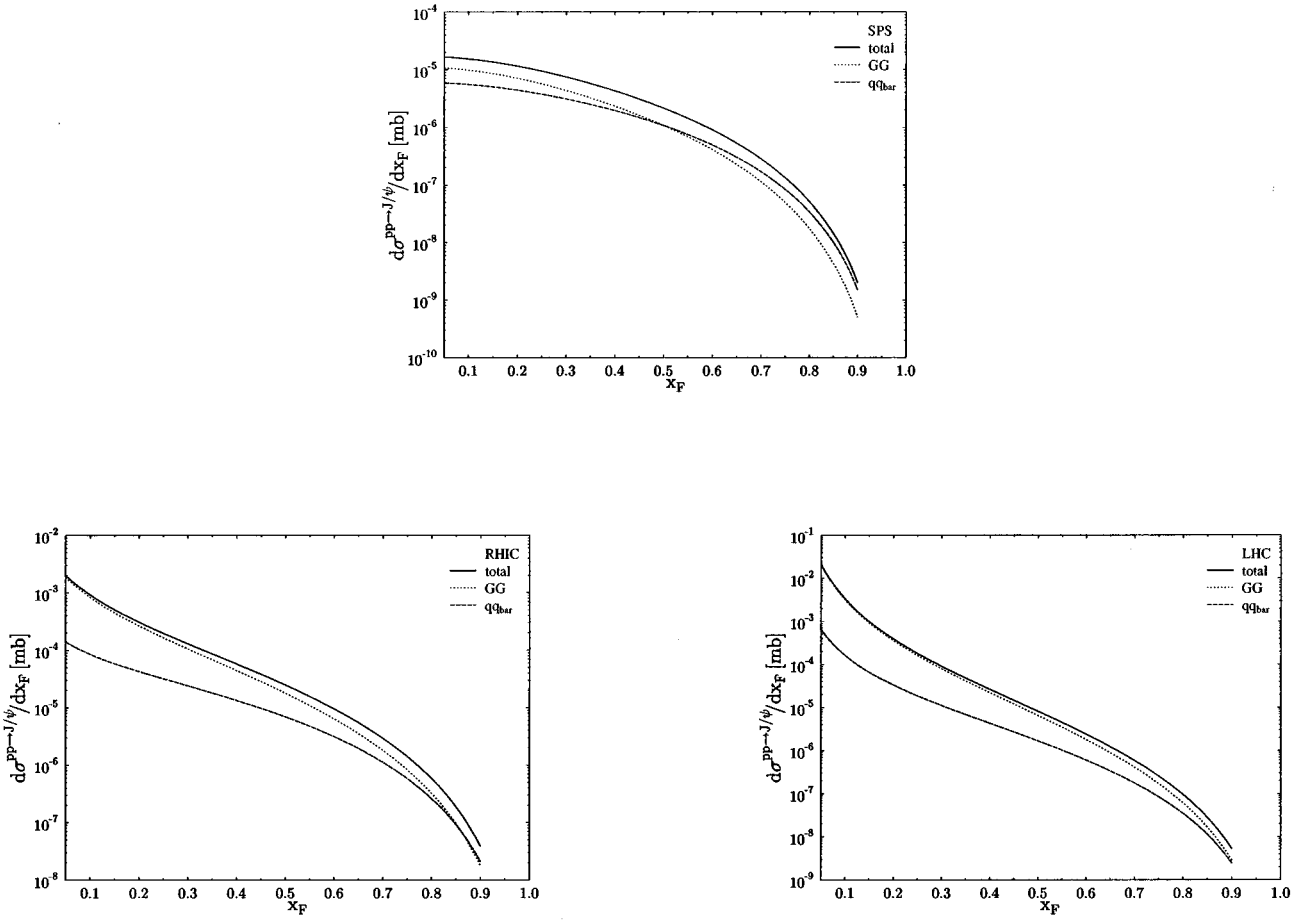

FIG. 9. $d\sigma^{pp\to J/\psi}/dx_F$ for SPS, RHIC, and LHC.

where $R=T(b)\sigma_{\rm eff}$. For the interaction of the $q\bar{q}$ pair one finds $\sigma_{{\rm eff},q\bar{q}}\approx 14$ mb, which approximately corresponds to the ρN cross section. We here assume that the perturbative factor 9/4 is valid also for the nonperturbative regime and, therefore, choose $\sigma_{{\rm eff},gg}\approx 30$ mb. At $b=0$ and for Pb one, therefore, has a maximum amount of shadowing of $A_{\rm eff}/A \approx 0.39$ which is approximately 15% smaller than the b-averaged result. Because the two different scenarios (lab- or infinite momentum frame) give such different results, $R_G\approx 0.39$ [25,26] vs $R_G\ll 0.3$ for heavy nuclei at small x, we decided to choose some intermediate value as a starting point for the DGLAP evolution.

We, therefore, employ the curves shown in Fig. 5 to account for the large difference in the quark and gluon shadowing ratios. Due to the large uncertainty of the initial R_G we choose the same ratio for Au and Pb at $Q^2=10$ GeV^2 as shown in Fig. 6. Also, we again want to emphasize that the commonly used shadowing ratios only account for impact-parameter-averaged measurements in DIS reactions. Therefore, our results should be seen as for central events only because the production mechanism in very peripheral collisions should produce significantly smaller rates with significantly smaller influences from shadowing effects [27].

For the minijet cross section we used a Q^2-dependent parametrization given in [16] to account for the larger p_T region.

V. RESULTS

We will first present the results for the minijet cross section including only processes $i,j\to k,l$ with $i,j=g$ and $k,l=q\bar{q}$ with four flavors in the final channel (due to the dominance of the gg fusion process annihilation processes are neglected at RHIC and LHC at midrapidity). For the x_F distribution we used our modified version of the parametrization in [11] but for the minijets we used an impact-parameter-dependent parametrization with $\mathbf{b}=0$ [16] shown in Fig. 7. This parametrization is applicable here since we are in the pure shadowing region where the generalized VMD approach used to derive it is applicable (even though one should say that the Glauber ansatz should only be valid up to values $x\sim 10^{-2}$ as restricted by the eikonal approximation).

The regions of the momentum fractions corresponding to the momentum range 1 GeV $<p_T<$ 6 GeV for RHIC ($\sqrt{s}=200$ GeV) and LHC ($\sqrt{s}=6$ TeV) are represented in Fig. 7 as shaded areas. The results for the cross sections for RHIC and LHC are given in Fig. 8. In that calculation all quark antiquark pairs ($k,l=q\bar{q}$) up to the bottom threshhold were taken into account, i.e., $N_f=4$ in the final state. One clearly sees the deviation having its origin in the shadowing of the nuclear parton distribution. As expected, the shadowing effect decreases as p_T increases due to the momentum fraction $x=2p_T/\sqrt{s}$.

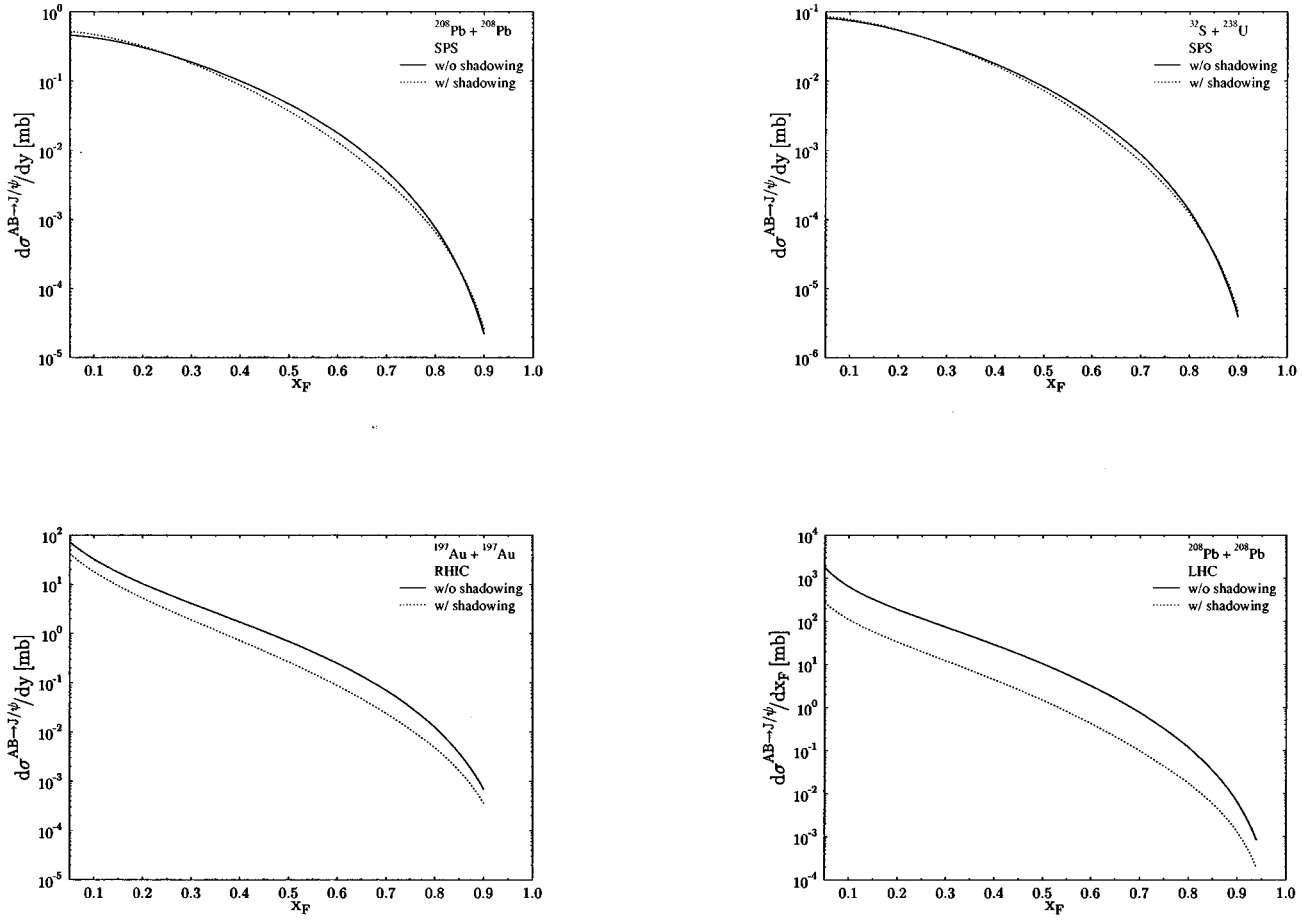

FIG. 10. $d\sigma^{AB\to J/\psi}/dx_F$ for SPS (Pb+Pb, $S+U$), RHIC (Au+Au), and LHC (Pb+Pb).

Next we will present the results for the $d\sigma^{AB}/dx_F$ cross sections. We first calculated the proton-proton cross sections to show the dominance of the gg fusion process over the $q\bar{q}$ annihilation process at small x_F (see Fig. 9): The results for the cross sections for $S+U$ and Pb+Pb at SPS at $\sqrt{s}=20$ GeV, Au+Au at RHIC at $\sqrt{s}=200$ GeV, and Pb+Pb at LHC at $\sqrt{s}=6$ TeV are presented in Fig. 10. In this case we were restricted to our modified version of the parametrization of [11] due to the integration reaching up to momentum fractions $x>0.1$, not allowing us to use the same parametrization as for the minijet production. At SPS energies one clearly sees the different regions of the parametrization entering the cross section. At small x_F one has the enhancement due to the antishadowing which is followed by the depletion due to the EMC region at larger x and finally one can identify the Fermi motion effect as $x_F\to 1$. The effects are clearly stronger for Pb+Pb than for $S+U$ (compare Fig. 4). To get an impression of the relative strength of the nuclear modifications in the respective nuclei we calculated the ratios of the shadowed to unshadowed cross sections in Fig. 11. The difference between Pb+Pb and $S+U$ at SPS energies in principle is only small; in the relevant region of small x_F, where the cross section has not dropped yet too much, the charmonium production in Pb+Pb is slightly larger than in $S+U(\approx 8\%)$. The RHIC one is in the shadowing region. The suppression strongly varies over the x_F range between ≈ 0.6 and 0.35. At LHC an even stronger suppression is found due to the smaller momentum fractions entering the shadowing ratios. Here the suppression is ≈ 0.3–0.5.

VI. CONCLUSIONS

From the results shown above one now can draw the following conclusions for the consequences of the shadowing effects for charmonium production and suppression in the energy regimes of SPS, RHIC, and LHC. First, one can conclude from Figs. 4 and 11 that an enhancement of charmonium states produced near midrapidity due to antishadowing at $\sqrt{s}=20$ GeV is predicted (small x_F). For larger x_F, a clear suppression of the charm cross section to ≈ 70–80% of the unshadowed result (Fig. 10) and again a rise at the largest x_F values is predicted (the latter one due to the Fermi motion effect).

For RHIC energies of $\sqrt{s}=200$ GeV the situation changes; for minijets with 1 GeV$<p_T<6$ GeV at midrapidity (or at small x_F, respectively) one is completely in the shadowing region. Here, the shadowed results are reduced by $\approx 45\%$. At LHC the situation is even more dramatic: the ratio of the shadowed cross section to the unshadowed cross section at $p_T=1$ GeV is 0.22 which amounts to a suppression of a factor ≈ 4.6.

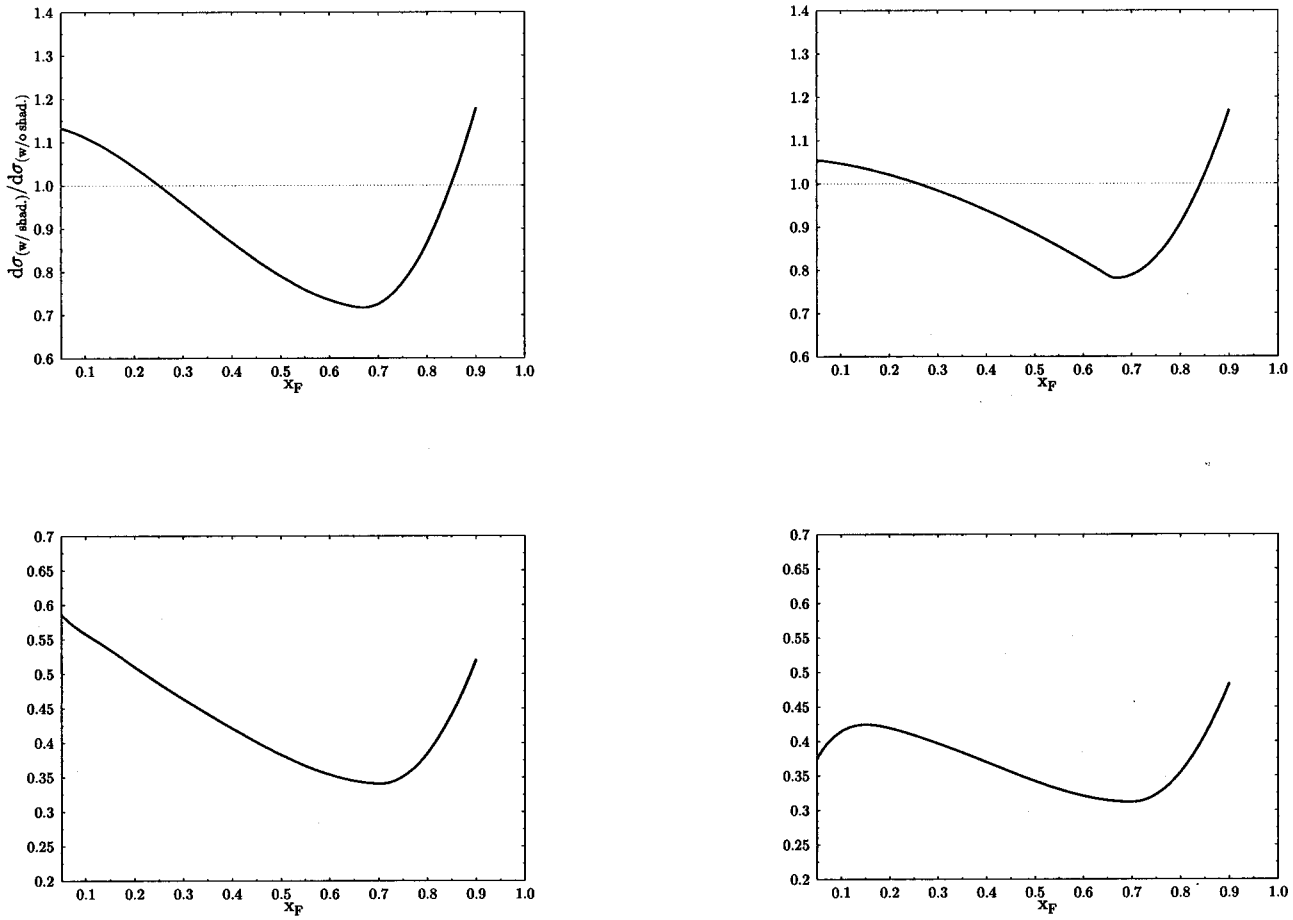

FIG. 11. $d\sigma^{AB\to J/\psi}_{\text{w/shad}}/dx_F/d\sigma^{AB\to J/\psi}_{w/o\ \text{shad}}/dx_F$ for SPS (Pb+Pb, $S+U$), RHIC (Au+Au), and LHC (Pb+Pb).

Similar effects are observable for $d\sigma^{AB\to J/\psi}/dx_F$: at small $x_F\approx 0.05$ for RHIC the cross section is reduced by a factor $d\sigma^{\text{shad}}/d\sigma^{\text{unshad}}\approx 0.58$, and gets suppressed even more towards larger x_F down to values ≈ 0.35. At LHC one finds a less strong variation over the x_F range with a mean value of ≈ 0.35. In these results one problem is unveiled: the difference between the (not yet exactly known) gluon ratio R_G and the quark ratio R_{F_2} that, according to the calulations in [24] increases with increasing mass number. If, as it was recently done at CERN-SPS, the future experiments at RHIC and LHC compare different combinations of nuclei and derive results similar to the NA50 data, one has to ask oneself whether one has detected the plasma or whether the detection is that the gluon ratio is *not simply* given by R_{F_2}, even at small x. This possibility becomes even more important since those initial-state interactions gain more influence as compared to SPS, even though one should say that the relative influence of the initial-state interactions as compared to the final-state interactions is not yet known exactly.

To give clear predictions, it is mandatory to control the value of R_G at the typical semihard scale $Q_{\text{SH}}\approx 2$ GeV with high precision. Therefore, charmonium and bottonium suppression effects can also be due to purely geometrical effects, i.e., shadowing.

ACKNOWLEDGMENTS

We gratefully appreciated discussions with L. Frankfurt and M. Strikman. This work was supported by BMBF, DFG, and GSI.

[1] C. Spieles, L. Gerland, N. Hammon, M. Bleicher, S. A. Bass, H. Stöcker, W. Greiner, C. Lourenço, and R. Vogt, Eur. Phys. J. A **1**, 51 (1998).

[2] N. Hammon, A. Dumitru, H. Stöcker, and W. Greiner, Phys. Rev. C **57**, 3292 (1998).

[3] R. C. Hwa, J. Pisut, and N. Pisutova, nucl-th/9706062.

[4] M. Gonin, NA50 Collaboration, Nucl. Phys. **A610**, 404c (1996); C. Lourenço, NA50 Collaboration, *ibid.* **A610**, 552c (1996).

[5] T. Matsui and H. Satz, Phys. Lett. B **178**, 416 (1986).

[6] D. Neubauer, K. Sailer, B. Müller, H. Stöcker, and W. Greiner, Mod. Phys. Lett. A **4**, 1627 (1989); S. Gavin, M. Gyulassy, and A. Jackson, Phys. Lett. B **207**, 257 (1988); S. Gavin and R. Vogt, Nucl. Phys. **B345**, 104 (1990); S. Gavin and R. Vogt,

Nucl. Phys. **A610**, 442c (1996); C. Gerschel and J. Huefner, hep-ph/9802245; C. Gerschel, J. Huefner, and E. Quack, J. Phys. G **22**, 1335 (1996).
[7] R. Gavai, D. Kharzeev, H. Satz, G. Schuler, K. Sridhar, and R. Vogt, hep-ph/9502270.
[8] G. A. Schuler, ''Quarkonium production and decays,'' CERN-preprint, CERN-TH.7170/94, 1997.
[9] L. Gerland, L. Frankfurt, M. Strikman, H. Stöcker, and W. Greiner, Phys. Rev. Lett. **81**, 762 (1998).
[10] J. J. Aubert *et al.*, Phys. Lett. **123B**, 275 (1983).
[11] K. J. Eskola, Nucl. Phys. **B400**, 240 (1993).
[12] M. Glück, R. Owens, and E. Reya, Phys. Rev. D **17**, 2324 (1978).
[13] D. O. Caldwell, Phys. Rev. D **7**, 1362 (1973); Phys. Rev. Lett. **42**, 553 (1979).
[14] L. Frankfurt and M. Strikman, Phys. Rep. **160**, 236 (1988).
[15] G. Piller, W. Ratzka, and W. Weise, Z. Phys. A **352**, 427 (1995).
[16] Z. Huang, H. J. Lu, and I. Sarcevic, hep-ph/9705250.
[17] L. Gribov, E. Levin, and M. Ryskin, Phys. Rep. **100**, 1 (1983).
[18] A. Müller and J. Qiu, Nucl. Phys. **B268**, 427 (1986).
[19] F. E. Close, J. Qiu, and R. G. Roberts, Phys. Rev. D **40**, 2820 (1989).
[20] L. Gerland, L. Frankfurt, M. Strikman, H. Stöcker, and W. Greiner, Phys. Rev. Lett. **81**, 762 (1998).
[21] D. M. Alde *et al.*, Phys. Rev. Lett. **64**, 2479 (1990).
[22] NM Collaboration, P. Amaudruz *et al.*, Z. Phys. C **51**, 387 (1991).
[23] R. G. Arnold *et al.*, Phys. Rev. Lett. **52**, 727 (1984).
[24] S. Kumano and K. Umekawa, hep-ph/9803359.
[25] L. Frankfurt, M. Strikman, and S. Liuti, ''Fourth Workshop on Experiments and Detectors for a Relativistic Heavy Ion Collider,'' BNL-Report BNL-52262, 1990.
[26] M. Strikman (private communication).
[27] V. Emel'yanov, A. Khodinov, S. R. Klein, and R. Vogt, hep-ph/9809222.